

Δ contributions to the parity-violating nuclear interaction

G. B. Feldman, G. A. Crawford, J. Dubach, and B. R. Holstein

Department of Physics and Astronomy, University of Massachusetts, Amherst, Massachusetts 01003

(Received 5 October 1990)

A quark-model picture which incorporates $SU(6)_w$ symmetry is utilized to calculate the weak Δ -nucleon-meson and Δ - Δ -meson parity-violating vertices for π , ρ , and ω mesons, thus extending previous work in the nucleon sector. The effective quark Hamiltonian is based upon the renormalization-group-corrected Weinberg-Salam model. The calculated parity-violating vertices are used to determine the coupling constants in an effective baryon Hamiltonian. We give "best" values as well as estimates of the ranges of uncertainty.

I. INTRODUCTION

Over the years nuclei have served as a crucial source of phenomenology for developing a deeper understanding of the weak interaction. Within the past decade, however, the Weinberg-Salam model has emerged as the accepted model of the electroweak interaction and the tables have turned toward using the weak interaction as a tool to aid in the understanding of hadrons and their interactions within nuclei. The most fundamental realization of the weak interaction in the purely hadronic sector is parity violation in the nucleon-nucleon interaction. Unfortunately, the Weinberg-Salam model, which is written in terms of quark and lepton degrees of freedom, is not easily applied to this problem since we still lack a reliable and calculable model by which to describe hadrons in terms of their quark-gluon degrees of freedom. Although QCD is widely believed to be the correct theory of the strong interaction, it is difficult to apply rigorously away from the high-energy perturbative region.

Nonetheless, there have been a number of attempts to describe the weak interaction between nucleons. Since the range of intermediate vector bosons is much smaller than the size of a nucleon, nucleons must be effectively overlapping in order to interact directly via W or Z exchange between quarks. Because the nucleon-nucleon interaction is repulsive at short distances, we expect such contributions to the parity-violating interaction to be small at low and medium energies. Thus most theoretical descriptions of parity violation in this energy regime have relied on the much longer-ranged exchange of light mesons (π , ρ , ω , etc.) between nucleons. In this case a simple one-meson-exchange weak nucleon-nucleon interaction is constructed with one nucleon-nucleon-meson (NNM) vertex being parity conserving and associated with the strong interaction, while the other is parity violating and arises from the weak force. All the weak-interaction physics is contained in this parity-violating NNM vertex. These vertices can be combined into an effective parity-violating nucleon-nucleon potential, which can be used to calculate parity-violating observables in this sector.¹

Such attempts have been generally successful in describing the available data, although in most cases

large theoretical uncertainties make it difficult to draw definitive conclusions. In recent years, for example, there has been considerable discussion of the weak $NN\pi$ coupling constant f_π —analyses^{2,3} of parity violation observed in experimental studies of electromagnetic transitions in ^{18}F , ^{19}F , and ^{21}Ne suggest a $NN\pi$ coupling considerably smaller than the "best value" given in the theoretical approach of Desplanques, Donoghue, and Holstein (DDH).⁴ Other theoretical models such as that of Dubovik and Zenkin⁵ or the soliton model of Kaiser and Meissner⁶ give considerably smaller values than DDH. However, all of these other values of f_π fall within the range of uncertainty estimated by DDH.

A measurement of particular current interest in testing such models is the longitudinal asymmetry in proton-proton scattering:

$$A_L = \frac{\sigma(+)-\sigma(-)}{\sigma(+)+\sigma(-)}, \quad (1)$$

where $\sigma(+)$ and $\sigma(-)$ are the total cross sections for scattering of protons with positive and negative helicity from an unpolarized target, respectively. In this reaction the largest contribution is usually expected to come from the vector mesons since the longer-range parity-violating pion exchange between protons is forbidden (neutral pions by Barton's theorem,⁷ charged pions by charge conservation). An experiment underway at TRIUMF⁸ at 230 MeV takes advantage of a cancellation between the 1S_0 and 3P_0 pp partial waves to emphasize the D -wave contribution and thus to isolate a different admixture of ρ - and ω -exchange contributions than occurs in the lower-energy measurements. Thus elastic proton-proton scattering offers the possibility of separating some of the various terms that contribute in the meson-exchange models, without the nuclear wave-function uncertainties which plague the ^{18}F , ^{19}F , and ^{21}Ne analysis.

Recently, however, Silbar *et al.*⁹ suggested that strongly produced virtual Δ 's may play an important role in the analysis of these proton-proton scattering experiments (see also Refs. 10 and 11). Since CP invariance allows a parity-violating $NN\pi^\pm$ vertex, they included such a term in the interaction combined with a strong $\Delta N\pi$ vertex and found the π -exchange contribution to be about 40% of the $(2.4 \pm 1.1) \times 10^{-7}$ asymmetry measured¹² at 800

MeV. More recent calculations¹³ with a different description of the strong-interaction physics obtained a smaller yet still very significant contribution. These estimates further suggest that a significant pion-exchange contribution may persist down into the energy regime of the TRIUMF experiment.

In order to be able to more fully assess the role played by the Δ in weak interactions within the hadronic sector, we have constructed parity-violating $N\Delta M$ and $\Delta\Delta M$ vertices with $M=\pi, \rho, \text{ and } \omega$. These vertices are calculated within the model originally developed by Desplanques, Donoghue, and Holstein⁴ for the NNM sector. This model employs a simple quark description of the baryons and mesons and uses an effective Weinberg-Salam model of the nonleptonic weak interactions which incorporates gluon-exchange renormalizations. This model and its extension into the Δ sector are described in the next section. In Sec. III we present our results in terms of effective couplings for NNM , $N\Delta M$, and $\Delta\Delta M$ vertices. The intent is to provide these results in a form which can readily be used within a coupled $N\Delta$ description of the strong-interaction dynamics such as that of Kloet and Silbar¹⁴ in order to calculate a parity-violating observable such as A_L (cf. Ref. 9). We conclude in Sec. IV with a brief summary of the model ingredients and the uncertainties which must be recognized in interpreting our results.

II. MODEL FOR THE WEAK VERTICES

The earliest calculations of nonleptonic parity-violating NNM vertices utilized very different techniques to evaluate the vector meson and pion couplings, with the former involving the use of factorization¹⁵ and the latter involving SU(3) plus partially conserved axial-vector current (PCAC) in order to relate the desired strangeness-conserving parity-violating pion vertices to measured hyperon decay amplitudes.¹⁶ An important step toward the goal of treating vector- and pseudoscalar-meson vertices on the same footing was taken by McKellar and Pick¹⁷ who applied SU(6)_w symmetry to the problem. Using this symmetry together with the Cabibbo (charged-current) Hamiltonian, it was possible to express the various desired $\Delta S=0$ NNM vertices in terms of five reduced matrix elements, three of which could be related to known parity-violating $\Delta S=1$ amplitudes. In 1980, Desplanques, Donoghue, and Holstein⁴ were able to extend and improve the formalism in two ways: (i) the two "unknown" reduced matrix elements were shown to correspond to calculable (modified) factorization diagrams, and (ii) the group-theoretical coupling factors were shown to arise from a simple quark-model picture of the process, allowing extension of this technique to neutral-current contributions, which could not be handled within the group-theoretical formalism without the introduction of additional reduced matrix elements. It is this formalism which has formed the basis of many of the nuclear parity-violation studies during the past decade and which therefore we choose to adapt to the calculation of ΔNM and $\Delta\Delta M$ weak vertices.

Although our procedure is quark-model based, it is

useful to review the group-theoretical language which was originally developed for the Cabibbo Hamiltonian by McKellar and Pick in order to relate our results to theirs and to those of DDH. The vector and pseudoscalar octet constitute a 35-dimensional representation of SU(6), while the charged-current pieces of $H^{PV}(\Delta S=1)$ and $H^{PV}(\Delta S=0)$ are members of common 35- and 280, $\overline{280}$ -dimensional representations. In the SU(6)_w approach one divides the full parity-violating Hamiltonian into two pieces:

$$H^{PV} = H_T^{PV} + H_V^{PV}, \quad (2)$$

where

$$H_T^{PV} \sim V_0 A_0 - V_3 A_3, \quad (3a)$$

$$H_V^{PV} \sim -\frac{1}{2}(V_- A_+ + V_+ A_-) \quad (3b)$$

are given in terms of longitudinal and transverse components of the product of the vector and axial-vector currents. It is then straightforward to enumerate the various ways by which to couple the two baryons and the meson together in a CP -invariant fashion:

$$[(\overline{BB})_{35} \otimes M_{35}]_{280, \overline{280}}, \quad (4a)$$

$$[(\overline{BB})_{405} \otimes M_{35}]_{280, \overline{280}}, \quad (4b)$$

$$[(\overline{BB})_{35} \otimes M_{35}]_{35}, \quad (4c)$$

leading to a group-theoretical picture involving five reduced matrix elements— a_T and a_V [for the coupling of Eq. (4a)], b_T and b_V [Eq. (4b)], and c_V [Eq. (4c)], where the subscript T or V indicates whether the origin of this term is from H_T or H_V , respectively.

Use of the quark model, besides allowing us to extend the range of validity of the group-theoretical methods, gives additional dynamical constraints. DDH demonstrated that the couplings of Eqs. (4) can be associated with the quark diagrams shown in Fig. 1. The fact that b_T and b_V can be related to a local four-quark matrix ele-

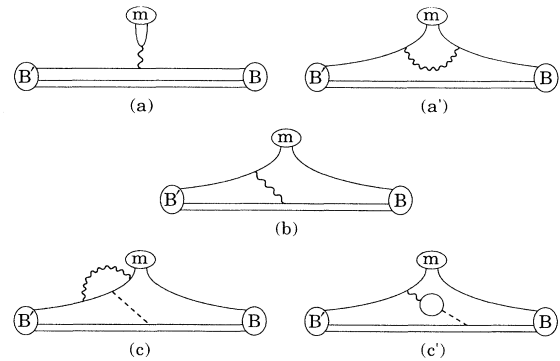


FIG. 1. Quark diagrams that are evaluated: (a) and (a') represent the factorization term discussed in Sec. II A, (b) the quark-model term of Sec. II B, and (c) and (c') the sum-rule term of Sec. II C. The solid lines represent the propagation of quarks, the dashed line that of a gluon, while the wavy lines represent the weak Hamiltonian.

ment implies by Lorentz covariance the relation $b_V = -b_T$. Also, since a_T and a_V correspond to the factorization diagrams, there exists in turn a relation between them which is simply a factor of $\frac{1}{3}$ introduced by color matching after a Fierz rearrangement, i.e., $a_T = a_V/3$. Thus the simplest unified description of $\Delta S = 0$ parity-violating vertices can be written in terms of just three independent reduced matrix elements. After the approximate incorporation of neutral-current effects, strong-interaction corrections, and SU(3) symmetry breaking, the model developed by DDH has eight independent parameters and can be straightforwardly generalized to calculate the $\Delta\Delta M$ and ΔNM vertices, as we shall show.

In order to describe the details of our calculation within the Δ sector, we briefly review the DDH procedure. Since we are not developing this technique in any novel fashion, we refer the reader to previous work for motivation and justification. The model is most easily described in terms of the diagrams shown in Fig. 1. In addition to the diagrams explicitly shown, the left-right mirror images of the diagrams in Figs. 1(b), 1(c), and 1(c') are implicitly included. The choice of diagrams and certain of the rules used to evaluate them are constrained to agree with the SU(6)_w results. In principle, by utilizing a quark-level weak Hamiltonian and a model for the quark structure of baryons, one could directly evaluate the baryon-baryon-meson vertices for each of these diagrams. However, the crudeness of models and methods for strong-interaction physics do not allow us to proceed so straightforwardly. Rather, the model of DDH utilizes a number of tricks which allow the evaluation of the needed diagrams in terms of only a few simple matrix elements which are determined empirically by fitting the $\Delta S = 1$ hyperon decay rates. We now proceed with a description of our calculation on a diagram-by-diagram basis.

A. Factorization diagram

The diagram in Fig. 1(a) represents the ‘‘factorization’’ contribution. The evaluation of this amplitude is straightforward and leads to a product of current matrix elements. The full weak Hamiltonian is quite complicated due to the inclusion of strong-interaction renormalization as discussed in Sec. IID. However, for purposes of illustration we can consider the quark Hamiltonian given by the charged Cabibbo model without strange quarks, i.e.,¹⁸

$$H_c^w(\Delta S = 0) = \frac{G}{\sqrt{2}} \cos^2 \theta_c \bar{d} \gamma_\mu (1 + \gamma_5) u \bar{u} \gamma^\mu (1 + \gamma_5) d, \quad (5)$$

where the $\bar{d}u$ pair is assumed to act at one quark vertex and the $\bar{u}d$ pair at the other (four-quark operators throughout this paper are assumed to be normal ordered). Since the parity-violating pion coupling from Fig. 1(a) vanishes in the SU(3) limit due to the conservation of the vector current, we consider the $n \rightarrow p\rho^-$ matrix element:

$$\langle p, \rho^- | H_c^{PV} | n \rangle_{(a)} = \frac{G}{\sqrt{2}} \cos^2 \theta_c \langle p | A_\mu^{1+i2} | n \rangle \times \langle \rho^- | V_{1-i2}^\mu | 0 \rangle, \quad (6)$$

where the axial-vector and vector current matrix elements are known from experiment.

Since a variety of other vertices can be related to that just examined within SU(6)_w, it is convenient to relate the product of current matrix elements in Eq. (6) to the reduced matrix elements of the SU(6)_w approach. The SU(6)_w couplings corresponding to the matrix elements a_T and a_V have the same transformation properties as the factorization diagram, and the relevant contribution to the $n \rightarrow p\rho^-$ vertex is the a_V term, which is given by⁴

$$\langle p, \rho^- | H_c^{PV} | n \rangle_{a_V} = \frac{10}{9} a_V \cot \theta_c. \quad (7)$$

Hence we obtain

$$a_V = \frac{9}{10} \frac{G}{\sqrt{2}} \cos \theta_c \sin \theta_c \langle p | A_\mu^{1+i2} | n \rangle \langle \rho^- | V_{1-i2}^\mu | 0 \rangle. \quad (8)$$

The charged-current Cabibbo Hamiltonian of Eq. (5) does not give rise to neutral meson vertices from the diagram of Fig. 1(a). However, a factorization contribution for neutral meson vertices can arise by considering the Fierz-rearranged Hamiltonian. This is equivalent to including the contribution from the diagram in Fig. 1(a'). For example, the Fierz-rearranged Hamiltonian corresponding to $H_c^w(\Delta S = 0)$ is given by

$$H_c^w(\Delta S = 0, \text{Fierz}) = \frac{G}{\sqrt{2}} \cos^2 \theta_c \bar{d}^i \gamma_\mu (1 + \gamma_5) d^j \bar{u}^j \gamma^\mu (1 + \gamma_5) u^i, \quad (9)$$

where we show explicitly the color indices which were previously suppressed. By evaluating the diagram in Fig. 1(a) using the Fierz-rearranged Hamiltonian, we obtain the contribution from the diagram in Fig. 1(a'). As an example, the factorization contribution to $p \rightarrow p\rho^0$ is

$$\langle p, \rho^0 | H_c^{PV} | p \rangle_{(a')} = -\frac{2}{3} \frac{G}{\sqrt{2}} \cos^2 \theta_c \langle p | A_\mu^3 | p \rangle \times \langle \rho^0 | V_3^\mu | 0 \rangle. \quad (10)$$

Evaluating this term and relating it to the SU(6)_w matrix elements in a fashion similar to that used in obtaining Eqs. (7) and (8), one may verify the relationship $a_T = a_V/3$.

The charged Cabibbo Hamiltonian contains a product of purely left-handed currents and upon Fierz rearrangement retains its left \otimes left form. However, because the Z couples to both right- and left-handed currents, both symmetric ($VA + AV$) and antisymmetric ($VA - AV$) products of currents enter. [It is the latter terms which prevent one from using the SU(6)_w group-theory formalism to calculate neutral-current contributions without introducing new reduced matrix elements.] Upon Fierz rearrangement the antisymmetric products produce a product of scalar and pseudoscalar densities, i.e.,

$VA - AV \rightarrow 2(SP - PS)$. Since the pseudoscalar operator can connect the vacuum to the π field, one must introduce a new parameter to represent such matrix elements in the factorization diagrams. The parameter defined in DDH for this purpose is

$$y \equiv 2 \langle \pi^- | \bar{d}^i \gamma_5 u^j | 0 \rangle \langle p | \bar{u}^j d^i | n \rangle \frac{G}{\sqrt{2}}, \quad (11)$$

which, applying the quark equations of motion and PCAC, can be written as

$$y = -i \frac{2}{3} \frac{GF_\pi m_\pi^2 S}{(m_u + m_d)}, \quad (12)$$

where $S = \langle p | \bar{u}d | n \rangle$.

By the use of quark-model symmetries among quark operators and baryon states, one can calculate all needed vertices from the factorization diagrams for any quark-model Hamiltonian which contains either $VA + AV$ or $VA - AV$ terms. The exact quark Hamiltonian used in this work will be described in the subsection on strong-interaction corrections.

Finally, as an example of a factorization diagram contribution to a vertex in the Δ sector, consider the contribution from the charged Cabibbo model to the vertex $\Delta^+(J_z = \frac{3}{2}) \rightarrow \Delta^{++}(J_z = \frac{1}{2}) + \rho^-(J_z = 1)$. [For all $B \rightarrow B' + M$ vertices discussed in this paper, the initial baryon and the meson will be assumed to have the maximum positive values of J_z .] The contribution from Fig. 1(a) is given by

$$\begin{aligned} & \langle \Delta^{++}, \rho^- | H_c^{PV} | \Delta^+ \rangle_{(a)} \\ &= \frac{G}{\sqrt{2}} \cos^2 \theta_c \langle \Delta^{++} | \bar{u} \gamma_\mu \gamma_5 d | \Delta^+ \rangle \langle \rho^- | \bar{d} \gamma^\mu u | 0 \rangle \\ &= \frac{G}{\sqrt{2}} \cos^2 \theta_c \langle \Delta^{++} | A_\mu^{1+i2} | \Delta^+ \rangle \langle \rho^- | V_{1-i2}^\mu | 0 \rangle, \end{aligned} \quad (13)$$

and by using the quark-model relationship

$$\langle \Delta^{++} | A_\mu^{1+i2} | \Delta^+ \rangle = \frac{3}{5} \langle p | A_\mu^{1+i2} | n \rangle, \quad (14)$$

we obtain

$$\langle \Delta^{++}, \rho^- | H_c^{PV} | \Delta^+ \rangle_{(a)} = \frac{2}{3} \cos \theta_c a_V. \quad (15)$$

Evaluation of factorization contributions involving π 's and ω 's proceeds similarly.

B. Quark-model diagram

Although we employed a quark-level Hamiltonian in our description of the factorization diagram [Fig. 1(a)], this was not really necessary since all calculations reduce to the evaluation of current matrix elements between hadrons. The use of a quark model does lead to the inclusion of the Fierz-rearranged terms discussed in the previous subsection [Fig. 1(a')]. However, the procedure for evaluating Fig. 1(a') is identical to that for Fig. 1(a) aside from a counting factor from color matching and is not dependent on details of the hadronic wave function.

TABLE I. Quark spin, flavor, and color wave functions used in the present work.

J_z	Δ^{++}	Δ^+	Δ^0	Δ^-
$\frac{3}{2}$	$\frac{1}{6} b_a^{\uparrow} b_b^{\uparrow} b_c^{\uparrow} \epsilon_{abc}$	$\frac{\sqrt{3}}{6} b_a^{\uparrow} b_b^{\uparrow} b_c^{\uparrow} \epsilon_{abc}$	$\frac{\sqrt{3}}{6} b_a^{\uparrow} b_b^{\uparrow} b_c^{\uparrow} \epsilon_{abc}$	$\frac{1}{6} b_a^{\uparrow} b_b^{\uparrow} b_c^{\uparrow} \epsilon_{abc}$
$\frac{1}{2}$	$\frac{\sqrt{3}}{6} b_a^{\uparrow} b_b^{\uparrow} b_c^{\uparrow} \epsilon_{abc}$	$\frac{1}{6} (b_a^{\uparrow} b_b^{\uparrow} b_c^{\uparrow} + 2b_a^{\uparrow} b_b^{\uparrow} b_c^{\uparrow}) \epsilon_{abc}$	$\frac{1}{6} (b_a^{\uparrow} b_b^{\uparrow} b_c^{\uparrow} + 2b_a^{\uparrow} b_b^{\uparrow} b_c^{\uparrow}) \epsilon_{abc}$	$\frac{\sqrt{3}}{6} b_a^{\uparrow} b_b^{\uparrow} b_c^{\uparrow} \epsilon_{abc}$
$\frac{1}{2}$	$\frac{1}{\sqrt{18}} (b_a^{\uparrow} b_b^{\uparrow} b_c^{\uparrow} - b_a^{\uparrow} b_b^{\uparrow} b_c^{\uparrow}) \epsilon_{abc}$	$\frac{1}{\sqrt{18}} (b_a^{\uparrow} b_b^{\uparrow} b_c^{\uparrow} - b_a^{\uparrow} b_b^{\uparrow} b_c^{\uparrow}) \epsilon_{abc}$	$\frac{1}{\sqrt{18}} (b_a^{\uparrow} b_b^{\uparrow} b_c^{\uparrow} - b_a^{\uparrow} b_b^{\uparrow} b_c^{\uparrow}) \epsilon_{abc}$	$\frac{1}{\sqrt{18}} (b_a^{\uparrow} b_b^{\uparrow} b_c^{\uparrow} - b_a^{\uparrow} b_b^{\uparrow} b_c^{\uparrow}) \epsilon_{abc}$
1	$\frac{\rho^+}{2b_l^{\uparrow} d_l^{\uparrow}}$	$\frac{\rho^0}{\sqrt{2}(b_l^{\uparrow} d_l^{\uparrow} - b_l^{\uparrow} d_l^{\uparrow})}$	$\frac{\rho^-}{2b_l^{\uparrow} d_l^{\uparrow}}$	$\frac{\omega}{\sqrt{2}(b_l^{\uparrow} d_l^{\uparrow} + b_l^{\uparrow} d_l^{\uparrow})}$
-1	$\frac{\rho^+}{2b_l^{\uparrow} d_l^{\uparrow}}$	$\frac{\rho^0}{\sqrt{2}(b_l^{\uparrow} d_l^{\uparrow} - b_l^{\uparrow} d_l^{\uparrow})}$	$\frac{\rho^-}{2b_l^{\uparrow} d_l^{\uparrow}}$	$\frac{\omega}{\sqrt{2}(b_l^{\uparrow} d_l^{\uparrow} + b_l^{\uparrow} d_l^{\uparrow})}$
0	$\frac{\pi^+}{\sqrt{2}(b_l^{\uparrow} d_l^{\uparrow} + b_l^{\uparrow} d_l^{\uparrow})}$	$(b_l^{\uparrow} d_l^{\uparrow} + b_l^{\uparrow} d_l^{\uparrow} - b_l^{\uparrow} d_l^{\uparrow} - b_l^{\uparrow} d_l^{\uparrow})$	$\frac{\pi^0}{(b_l^{\uparrow} d_l^{\uparrow} + b_l^{\uparrow} d_l^{\uparrow} - b_l^{\uparrow} d_l^{\uparrow} - b_l^{\uparrow} d_l^{\uparrow})}$	$\frac{\pi^-}{\sqrt{2}(b_l^{\uparrow} d_l^{\uparrow} + b_l^{\uparrow} d_l^{\uparrow})}$

The remaining diagrams of Fig. 1, however, are directly sensitive to the details of hadronic structure.

The diagram in Fig. 1(b) is termed the “quark-model diagram,” and its evaluation requires the quark-model spin, flavor, and color wave functions of the hadrons involved; we list these in Table I to explicitly define our conventions. We assume that the quarks are in S -wave states. Then, as we will show below, we do not need to know details of the spatial wave functions, since the radial integral is just a common factor for all vertices in the $SU(6)$ limit. We need not explicitly evaluate this integral. Rather, we determine it empirically from fits to parity-violating hyperon decay data.

Given a weak quark Hamiltonian, to evaluate the diagram of Fig. 1(b) one calculates matrix elements of the form

$$\langle 0 | \epsilon^{ijk} (b^k b^j b^i) (d^l b^l) \bar{q} \gamma_\mu \gamma_5 q \bar{q} \gamma^\mu q (b^{\dagger m} b^{\dagger n} b^{\dagger o}) \epsilon^{mno} | 0 \rangle . \quad (16)$$

Here $\epsilon^{ijk} (b^k b^j b^i)$ comes from the final baryon, $(d^l b^l)$ from the meson, $\bar{q} \gamma_\mu \gamma_5 q \bar{q} \gamma^\mu q$ is the four-quark operator

from the Hamiltonian, and $(b^{\dagger m} b^{\dagger n} b^{\dagger o}) \epsilon^{mno}$ generates the initial baryon. When we take the contractions of the quark creation and annihilation operators appropriate to the diagram of Fig. 1(b), we are left with c numbers multiplied by spin matrix elements $\chi^\dagger \chi_3 \chi_2^\dagger \chi_4$ or $\chi_1^\dagger \sigma \chi_3 \cdot \chi_2^\dagger \sigma \chi_4$. For each baryon-baryon-meson vertex, we must sum over the spins of the four interacting quarks. This is done for each term in the Hamiltonian as well as for each term in the baryon wave functions.

A subtlety in this calculation involves the inclusion of an additional diagram which is the left-right mirror image of the diagram in Fig. 1(b). As is discussed in DDH, because of crossing symmetry, this diagram can be included in a way consistent with $SU(6)_w$ by calculating an absorption diagram, i.e., $\langle B' | H^{\text{PV}} | BM \rangle$. For vector meson vertices the absorption diagrams must be added to the emission diagrams for consistency with $SU(6)_w$, while for pion vertices they must be subtracted. A similar procedure will be applied to the diagrams of Figs. 1(c) and 1(c') as discussed in the next subsection.

As an example of such an evaluation, we will consider the contribution from the charged Cabibbo model to the vertex $\Delta^{++} \rightarrow \Delta^+ + \rho^+$:

$$\begin{aligned} \langle \Delta^+ \rho^+ | H_c^{\text{PV}} | \Delta^{++} \rangle_{(b)} &= \frac{G}{\sqrt{2}} \cos^2 \theta_c \langle 0 | \frac{1}{6} \epsilon^{ijk} (b_k^\dagger b_j^\dagger b_i^\dagger + 2b_k^\dagger b_j^\dagger b_i^\dagger) (2d_l^\dagger b_l^\dagger) (\bar{u} \gamma_\mu \gamma_5 d \bar{d} \gamma^\mu u + \bar{u} \gamma_\mu d \bar{d} \gamma^\mu \gamma_5 u) \\ &\quad \times \frac{1}{6} \epsilon^{abc} (b_a^\dagger u^\dagger b_b^\dagger u^\dagger b_c^\dagger u^\dagger) | 0 \rangle \\ &= \mathcal{C} \frac{2}{3} \epsilon^{ijk} \epsilon^{abc} \delta_{ic} \delta_{jb} \delta_{ka} [\chi^\dagger(\uparrow) \chi(\downarrow) \chi^\dagger(\downarrow) \chi(\uparrow) - \chi^\dagger(\uparrow) \sigma \chi(\downarrow) \cdot \chi^\dagger(\downarrow) \sigma \chi(\uparrow) \\ &\quad + \chi^\dagger(\downarrow) \chi(\downarrow) \chi^\dagger(\uparrow) \chi(\uparrow) - \chi^\dagger(\downarrow) \sigma \chi(\downarrow) \cdot \chi^\dagger(\uparrow) \sigma \chi(\uparrow)] \\ &= -4\mathcal{C} [\chi^\dagger(\uparrow) \chi(\downarrow) \chi^\dagger(\downarrow) \chi(\uparrow) - \chi^\dagger(\uparrow) \sigma \chi(\downarrow) \cdot \chi^\dagger(\downarrow) \sigma \chi(\uparrow) \\ &\quad + \chi^\dagger(\downarrow) \chi(\downarrow) \chi^\dagger(\uparrow) \chi(\uparrow) - \chi^\dagger(\downarrow) \sigma \chi(\downarrow) \cdot \chi^\dagger(\uparrow) \sigma \chi(\uparrow)] , \end{aligned} \quad (17)$$

where \mathcal{C} is a product of constants and the radial integral, which we take to be identical for all vertices which we consider. Since H_V^{PV} of Eqs. (2), (3a), and (3b) requires a spin flip, while H_T^{PV} does not, the first two terms in Eq. (17) correspond to H_V^{PV} , while the latter two terms correspond to H_T^{PV} . It can be seen that for the mirror image absorption diagram there can be no charged-current contribution for this vertex. Then, by comparing Eq. (17) to the $SU(6)_w$ predictions,

$$\langle \Delta^+ \rho^+ | H_c^{\text{PV}} | \Delta^{++} \rangle_{(b_T)} = \frac{1}{3} b_T , \quad (18a)$$

$$\langle \Delta^+ \rho^+ | H_c^{\text{PV}} | \Delta^{++} \rangle_{(b_V)} = \frac{1}{3} b_V , \quad (18b)$$

we obtain the relationships

$$b_T = -12\mathcal{C} [\chi^\dagger(\downarrow) \chi(\downarrow) \chi^\dagger(\uparrow) \chi(\uparrow) - \chi^\dagger(\downarrow) \sigma \chi(\downarrow) \cdot \chi^\dagger(\uparrow) \sigma \chi(\uparrow)] \cot \theta_c = -24\mathcal{C} \tan \theta_c , \quad (19a)$$

$$b_V = -12\mathcal{C} [\chi^\dagger(\uparrow) \chi(\downarrow) \chi^\dagger(\downarrow) \chi(\uparrow) - \chi^\dagger(\uparrow) \sigma \chi(\downarrow) \cdot \chi^\dagger(\downarrow) \sigma \chi(\uparrow)] \cot \theta_c = 24\mathcal{C} \tan \theta_c = -b_T . \quad (19b)$$

The value of \mathcal{C} can be obtained from measured parity-violating hyperon decay amplitudes, and with it we can evaluate the diagram of Fig. 1(b) for all remaining baryon-baryon-meson vertices of interest.

C. Sum-rule diagram

The last diagrams to be considered are shown in Figs. 1(c) and 1(c') and are related to the pion “sum-rule” calculation.⁴ There is no clear technique for evaluating this contribution in the quark model since it directly involves strong-interaction effects. The prescription adopted by DDH is to contract two quark lines in the Hamiltonian to represent the virtual quark-antiquark pair inside the nucleon and insert an $SU(3)$ color matrix. Thus the four-quark operator becomes an effective two-quark operator, i.e., $\bar{q}^i q^i \bar{q}^j q^j \rightarrow \bar{q}^i q^j \Lambda^{ij}$.

The diagram of Fig. 1(c') is equivalent to that of Fig. 1(c) for a Fierz-rearranged Hamiltonian. Looking at Fig. 1(c'),

its contribution would seem to be zero since $\text{Tr}\Lambda=0$. However, gluonic renormalization leads to terms in an effective Weinberg-Salam Hamiltonian which result from the exchange of a gluon parallel to the W and Z bosons. (We will discuss gluonic renormalization in Sec. II D.) As was the case for the factorization diagram, Fierz rearrangement of the $VA - AV$ terms in the Hamiltonian leads to a new parameter ξ , which is defined as

$$\xi \equiv \frac{\langle B'M|2(SP-PS)|B \rangle_{(c)}}{\langle B'M|(VA-AV)|B \rangle_{(c)}}. \quad (20)$$

As an example of a sum-rule diagram calculation, we will consider the contribution from the charged Cabibbo model to the vertex $\Delta^{++}(J_z=\frac{3}{2}) \rightarrow \Delta^+ + \rho^+$. This time we cannot ignore the strange quarks in the Hamiltonian because it is possible for the intermediate $\bar{q}q$ in Fig. 1(c) to be an $s\bar{s}$ pair. Thus the Hamiltonian that we use is

$$H_c^w(\Delta S=0) = \frac{G}{\sqrt{2}} [\cos^2\theta_c \bar{d}\gamma_\mu(1+\gamma_5)u\bar{u}\gamma^\mu(1+\gamma_5)d + \sin^2\theta_c \bar{s}\gamma_\mu(1+\gamma_5)u\bar{u}\gamma^\mu(1+\gamma_5)s]. \quad (21)$$

It is straightforward to see that the resulting effective two-quark operators are $(\bar{u}u + \bar{d}d)\cos^2\theta_c$ and $\bar{u}u\sin^2\theta_c$. Only $\bar{d}d$ can contribute to the diagram in Fig. 1(c) and only $\bar{u}u$ to the corresponding absorption diagram. In the former case the result is proportional to

$$\begin{aligned} \frac{G}{\sqrt{2}} \cos^2\theta_c \langle 0 | \frac{1}{6} \epsilon^{ijk} (b_k^{u\uparrow} b_j^{u\uparrow} b_i^{d\downarrow} + 2b_k^{u\uparrow} b_j^{u\downarrow} b_i^{d\uparrow}) (2d_l^{d\uparrow} b_l^{u\uparrow}) \bar{d} \mathcal{O} d \frac{1}{6} \epsilon^{abc} (b_a^{t\uparrow} b_b^{t\uparrow} b_c^{t\uparrow}) | 0 \rangle \\ = \frac{G}{\sqrt{2}} \frac{1}{3} \epsilon^{abc} \epsilon^{ijk} \delta_{ic} \delta_{jb} \delta_{ka} \cos^2\theta_c \langle \mathcal{O} \rangle = -\sqrt{2} G \cos^2\theta_c \langle \mathcal{O} \rangle, \end{aligned} \quad (22)$$

while for the latter we obtain

$$\begin{aligned} (\cos^2\theta_c + \sin^2\theta_c) \langle 0 | \frac{1}{6} \epsilon^{ijk} (b_k^{u\uparrow} b_j^{u\uparrow} b_i^{d\downarrow} + 2b_k^{u\uparrow} b_j^{u\downarrow} b_i^{d\uparrow}) \bar{u} \mathcal{O} u (2b_l^{t\downarrow} d_l^{t\uparrow}) \frac{1}{6} \epsilon^{abc} (b_a^{t\uparrow} b_b^{t\uparrow} b_c^{t\uparrow}) | 0 \rangle \\ = \frac{G}{\sqrt{2}} \frac{1}{3} \epsilon^{abc} \epsilon^{ijk} \delta_{ic} \delta_{jb} \delta_{ka} (\cos^2\theta_c + \sin^2\theta_c) \langle \mathcal{O} \rangle = -\sqrt{2} G (\cos^2\theta_c + \sin^2\theta_c) \langle \mathcal{O} \rangle. \end{aligned} \quad (23)$$

Here \mathcal{O} is an unknown operator which represents the contraction into a two-quark operator. $\langle \mathcal{O} \rangle$ is thus an unknown matrix element, but it will be the same for all of the vertices that we consider. Adding these two contributions, we have

$$\langle \Delta^+, \rho^+ | H_c^{\text{PV}} | \Delta^{++} \rangle_{(c)} = -\sqrt{2} G (2\cos^2\theta_c + \sin^2\theta_c) \langle \mathcal{O} \rangle. \quad (24)$$

Using the $\text{SU}(6)_w$ prediction

$$\langle \Delta^+, \rho^+ | H_c^{\text{PV}} | \Delta^{++} \rangle_{(c_V)} = -(\frac{2}{3}\cot\theta_c + \frac{1}{3}\tan\theta_c) c_V, \quad (25)$$

we identify

$$c_V = 3\sqrt{2} G \cos\theta_c \sin\theta_c \langle \mathcal{O} \rangle. \quad (26)$$

Thus we are able to evaluate the common factor $\langle \mathcal{O} \rangle$ in terms of the reduced matrix element c_V and hence to evaluate the sum-rule diagram for all other vertices of interest.

D. Strong-interaction effects

The Weinberg-Salam model has proven to be a remarkably successful theory for the electroweak interaction. One can obtain an effective four-quark Hamiltonian with the Weinberg-Salam model by integrating out the intermediate vector bosons, and it is such a Hamiltonian that we have considered to this point. However, this is not totally appropriate in the hadronic sector where strong-interaction effects can be considerable. To try to take such effects into account, we use an effective Hamiltonian based on the Weinberg-Salam model, but modified to include gluonic renormalizations through the use of Wilson's operator product expansion¹⁹ and renormalization-group techniques.^{20,21} In the notation of DDH, this effective Hamiltonian is

$$\begin{aligned} H_{\text{WS}}^{\text{eff}}(\Delta S=0) = \frac{G}{\sqrt{2}} \cos\theta_c \sin\theta_c \left\{ \sum_{i=1}^2 [\alpha_{ii} \mathcal{O}(A_i^\dagger, A_i) + \beta_{ii} \mathcal{O}(A_i^\dagger t^A, A_i t^A) + \text{H.c.}] \right. \\ \left. + \sum_{i,j=1}^2 [\gamma_{ij} \mathcal{O}(B_i, B_j) + \delta_{ij} \mathcal{O}(B_i t^A, B_j t^A)] \right\}, \end{aligned} \quad (27)$$

where

$$O(M, N) \equiv \bar{q} \gamma_\mu \gamma_5 M q \bar{q} \gamma^\mu N q, \quad (28)$$

$$q \equiv \begin{pmatrix} u \\ d \\ s \end{pmatrix}, \quad (29)$$

$$A_1 \equiv \begin{pmatrix} 0 & 1 & 0 \\ 0 & 0 & 0 \\ 0 & 0 & 0 \end{pmatrix}, \quad A_2 \equiv \begin{pmatrix} 0 & 0 & 1 \\ 0 & 0 & 0 \\ 0 & 0 & 0 \end{pmatrix},$$

$$B_1 \equiv \begin{pmatrix} 1 & 0 & 0 \\ 0 & 1 & 0 \\ 0 & 0 & 1 \end{pmatrix}, \quad B_2 \equiv \begin{pmatrix} 1 & 0 & 0 \\ 0 & -1 & 0 \\ 0 & 0 & -1 \end{pmatrix}, \quad (30)$$

and the t^A are SU(3) color matrices normalized to

$$\text{Tr } t^A t^B = 2\delta^{AB}. \quad (31)$$

The α 's, β 's, γ 's, and δ 's are functions of a parameter which depends on the strong-interaction coupling constant and renormalization scale and is defined as

$$K \equiv 1 + \frac{g^2(\mu^2)}{16\pi^2} b \ln \left[\frac{M_W^2}{\mu^2} \right], \quad (32)$$

where g is the color gluon coupling constant, μ is the renormalization point, and $b = 11 - \frac{2}{3}N$, with N the number of quark flavors. In terms of this parameter, we have⁴

$$\alpha_{11} = \cot\theta_c (K^{0.48} + 2K^{-0.24})/3, \quad (33a)$$

$$\alpha_{22} = \tan^2\theta_c \alpha_{11}, \quad (33b)$$

$$\beta_{11} = \cot\theta_c (-K^{0.48} + K^{-0.24})/4, \quad (33c)$$

$$\beta_{22} = \tan^2\theta_c \beta_{11}, \quad (33d)$$

$$\frac{1}{2}\sin 2\theta_c \gamma_{11} = (3 - 2\sin^2\theta_w)(0.056K^{0.48} - 0.051K^{0.35} - 0.067K^{-0.24} + 0.062K^{-0.40}), \quad (33e)$$

$$\frac{1}{2}\sin 2\theta_c \gamma_{12} = -\frac{1}{3}\sin\theta_w (-0.049K^{0.85} + 0.190K^{0.43} - 0.426K^{-0.13} + 0.274K^{-0.35}), \quad (33f)$$

$$\frac{1}{2}\sin 2\theta_c \gamma_{21} = -\frac{1}{3}\sin\theta_w (0.086K^{0.85} + 0.146K^{0.43} + 0.623K^{-0.13} + 0.151K^{-0.35}), \quad (33g)$$

$$\frac{1}{2}\sin 2\theta_c \gamma_{22} = (1 - 2\sin^2\theta_w)(0.167K^{0.48} + 0.333K^{-0.24}), \quad (33h)$$

$$\frac{1}{2}\sin 2\theta_c \delta_{11} = (3 - 2\sin^2\theta_w)(-0.042K^{0.48} + 0.028K^{0.35} - 0.025K^{-0.24} + 0.039K^{-0.40}), \quad (33i)$$

$$\frac{1}{2}\sin 2\theta_c \delta_{12} = -\frac{1}{3}\sin\theta_w (-0.113K^{0.85} - 0.099K^{0.43} + 0.129K^{-0.13} + 0.079K^{-0.35}), \quad (33j)$$

$$\frac{1}{2}\sin 2\theta_c \delta_{21} = -\frac{1}{3}\sin\theta_w (0.063K^{0.85} - 0.126K^{0.43} - 0.084K^{-0.13} + 0.148K^{-0.35}), \quad (33k)$$

$$\frac{1}{2}\sin 2\theta_c \delta_{22} = (1 - 2\sin^2\theta_w)(-K^{0.48} + K^{-0.24})/8. \quad (33l)$$

We can recover the simple Weinberg-Salam Hamiltonian in the absence of strong interaction effects by taking $K=1$ ($g=0$). In this limit, $\delta_{ij}=\beta_{ii}=\gamma_{11}=\gamma_{12}=0$ for all i, j , and the remaining terms simplify to $\alpha_{11}=\cot\theta_c$, $\alpha_{22}=\tan\theta_c$, $\gamma_{21}=-\frac{2}{3}\sin^2\theta_w \csc 2\theta_c$, and $\gamma_{22}=(1-2\sin^2\theta_w)\csc 2\theta_c$.

The four-quark operators which multiply each of the coefficients α_{11} , α_{22} , etc., can readily be obtained from Eq. (27); for example, the coefficient α_{11} multiplies the combination of operators $\bar{u}^i \gamma_\mu \gamma_5 d^i \bar{d}^j \gamma^\mu u^j + \bar{d}^i \gamma_\mu \gamma_5 u^i \bar{u}^j \gamma^\mu d^j$. Note that the β_{ii} and δ_{ij} terms in the Hamiltonian contain SU(3) color matrices and exist as a consequence of a gluonic renormalization in which a

gluon is exchanged parallel to the vector gauge boson. The β_{ii} and δ_{ij} terms multiply combinations of four-quark operators with the same flavor indices as do the α_{ii} and γ_{ij} , respectively, but their color indices differ. One can obtain the relevant four-quark operators multiplying the β and δ terms by replacing $\bar{q}^i q^i \bar{q}^j q^j$ with $2\bar{q}^i q^j \bar{q}^j q^i - \frac{2}{3}\bar{q}^i q^i \bar{q}^j q^j$ in the α and γ terms, respectively. For example, the β_{11} coefficient multiplies the combination of operators $\bar{u}^i d^j \bar{d}^j u^i - \frac{2}{3}\bar{u}^i d^i \bar{d}^j u^j + \bar{d}^i u^j \bar{u}^j d^i - \frac{2}{3}\bar{d}^i u^i \bar{u}^j d^j$. Thus our effective Hamiltonian is written as a series of four-quark operators and the techniques of Secs. II A–II C can be applied in order to evaluate any required NNM , ΔNM , or $\Delta\Delta M$ vertex.

III. RESULTS

At this point we are in a position to evaluate the five diagrams of Fig. 1 (and the corresponding absorption diagrams) for all $\Delta S=0$ S -wave vertices involving Δ 's in terms of the parameters $a_T, a_V, b_T, b_V, c_V, y, K$, and ξ . We list general expressions for 11 independent vertices in Table II. Any other matrix elements may be obtained from these as may the coupling constants of the effective weak Hamiltonian that we introduce below. The $\alpha_{ij}, \beta_{ij}, \gamma_{ij}$, and δ_{ij} that appear in Table II are the functions of K defined in Sec. II D. The α_{ij} and β_{ij} terms correspond to charged-current contributions, while γ_{ij} and δ_{ij} represent neutral-current contributions. If one sets $K=1$ (no strong-interaction renormalization) and $\gamma_{ij}=\delta_{ij}=0$ (no neutral currents), Table II reduces to the $SU(6)_w$ results that one would obtain using the effective Hamiltonian¹⁷ of McKellar and Pick.

As discussed in Sec. II A, the parameter y appears only in the pionic vertex, while the parameters a_T and a_V only appear for vector-meson vertices. All the vector-meson vertices are calculated for the $J_z=1$ case. From Eqs. (3a) and (3b), one can see that H_V^{PV} corresponds to the exchange of weak gauge bosons with $J_z=\pm 1$, while H_T^{PV} corresponds to $J_z=0$ exchange. The a_T terms in Table II result solely from the evaluation of the diagram of Fig.

1(a') and the a_V terms from that of Fig. 1(a).

The reduced matrix elements a_T, a_V, b_T, b_V , and c_V , being defined in terms of hyperon decay, all have an identical $\cos\theta_c \sin\theta_c$ dependence on the Cabibbo angle. It is then easy to see that in Table II the charged-current terms [α_{ii} and β_{ii} of Eq. (29)] and the neutral-current terms (γ_{ij} and δ_{ij}) have the proper θ_c dependence.

As was discussed in Sec. II D, some of the terms in the effective Weinberg-Salam Hamiltonian [β_{ii} and δ_{ij} of Eq. (29)] contain $SU(3)$ color matrices. These terms exist as a consequence of strong-interaction renormalization. For the contribution of four of the five diagrams of Fig. 1 to the baryon-baryon-meson matrix elements, the coefficients multiplying the β_{ii} and the δ_{ij} terms are not independent of those multiplying the α_{ii} and γ_{ii} terms, respectively—i.e., the contribution from these diagrams can be written in terms of linear combinations of α_{ii} and β_{ii} and of γ_{ij} and δ_{ij} . In Table II we have adopted shorthand notation for these combinations, i.e., $A_{ij}=\alpha_{ij}+\frac{16}{3}\beta_{ij}$. Figure 1(c') is the exception where, as was stated in Sec. III C, the contribution from this diagram would be zero without gluonic renormalization of the Weinberg-Salam Hamiltonian.

The amplitudes for the baryon-baryon-meson vertices can be used to determine effective coupling constants in the effective weak parity-violating Hamiltonian:

$$\begin{aligned}
H_{NN\pi}^{PV} &= \frac{1}{\sqrt{2}} f_{NN\pi} \bar{\psi}(\tau \times \phi^\pi)_0 \psi, \\
H_{NN\omega}^{PV} &= \bar{\psi}(h_{NN\omega}^0 \phi_\nu^\omega + h_{NN\omega}^1 \tau_0 \phi_\nu^\omega) \gamma^5 \psi, \\
H_{NN\rho}^{PV} &= \bar{\psi}[h_{NN\rho}^0 \tau \cdot \phi_\nu^\rho + h_{NN\rho}^1 \phi_{\nu 0}^\rho + h_{NN\rho}^2 (3\tau_0 \phi_{\nu 0}^\rho - \tau \cdot \phi_\nu^\rho) / 2\sqrt{6}] \gamma^5 \psi, \\
H_{\Delta N\omega}^{PV} &= h_{\Delta N\omega}^1 \bar{\psi} \phi_\mu^\omega \Psi^{\mu 0} + \text{H.c.}, \\
H_{\Delta N\rho}^{PV} &= h_{\Delta N\rho}^0 \bar{\psi} \phi_{\mu i}^\rho \Psi^{\mu i} + h_{\Delta N\rho}^1 \bar{\psi} \phi_{\mu 0}^\rho \Psi^{\mu 0} + h_{\Delta N\rho}^{\prime 1} (\bar{\psi} \phi_{\mu+}^\rho \Psi^{\mu-} - \bar{\psi} \phi_{\mu-}^\rho \Psi^{\mu+} - \bar{\psi} \tau^i \phi_{\mu i}^\rho \Psi^{\mu 0}) + \text{H.c.}, \\
H_{\Delta\Delta\pi}^{PV} &= \frac{1}{\sqrt{2}} f_{\Delta\Delta\pi} \bar{\Psi}^{\mu i} (\tau \times \phi^\pi)_0 \Psi_{\mu i}, \\
H_{\Delta\Delta\omega}^{PV} &= \bar{\Psi}^{\mu i} (h_{\Delta\Delta\omega}^0 \phi_\nu^\omega + h_{\Delta\Delta\omega}^1 \tau_0 \phi_\nu^\omega) \gamma^5 \Psi_{\mu i}, \\
H_{\Delta\Delta\rho}^{PV} &= \bar{\Psi}^{\mu i} [h_{\Delta\Delta\rho}^0 \tau \cdot \phi_\nu^\rho + h_{\Delta\Delta\rho}^1 \phi_{\nu 0}^\rho + h_{\Delta\Delta\rho}^2 (3\tau_0 \phi_{\nu 0}^\rho - \tau \cdot \phi_\nu^\rho) / 2\sqrt{6}] \gamma^5 \Psi_{\mu i} \\
&\quad + h_{\Delta\Delta\rho}^{\prime 1} (\bar{\Psi}^{\mu+} \tau^- \phi_{\nu i}^\rho \gamma^5 \Psi_{\mu i} - \bar{\Psi}^{\mu-} \tau^+ \phi_{\nu i}^\rho \gamma^5 \Psi_{\mu i} + \text{H.c.}),
\end{aligned} \tag{34}$$

where $\Psi^{\mu i}$ is a Rarita-Schwinger spinor with μ the time-space index and i the isospin index, ψ is the nucleon Dirac spinor, and $\phi^\pi, \phi_\nu^\omega$, and ϕ_ν^ρ are the field operators for the π, ω , and ρ fields, respectively. The $\Delta\Delta M$ Hamiltonian looks very similar to the NNM Hamiltonian⁴ with the Dirac spinors replaced by Rarita-Schwinger spinors. One new term $h_{\Delta\Delta\rho}^{\prime 1}$ enters, but only the isovector neutral-current terms in the diagram of Fig. 1(b) contribute to it, and it is, therefore, small. This term is the only contribution to the $\Delta\Delta M$ Hamiltonian from the diagram of Fig. 1(b).

The coupling constants of the hadronic Hamiltonian are related to the 11 vertices in Table II by the following relationships:

$$h_{\Delta N\omega}^1 = \sqrt{\frac{3}{2}} \langle p\omega | H^{PV} | \Delta^+ \rangle, \tag{35a}$$

$$h_{\Delta N\rho}^0 = \frac{1}{2} (\langle n\rho^- | H^{PV} | \Delta^- \rangle - \langle p\rho^+ | H^{PV} | \Delta^{++} \rangle), \tag{35b}$$

$$h_{\Delta N\rho}^{\prime 1} = -\frac{1}{2} (\langle n\rho^- | H^{PV} | \Delta^- \rangle + \langle p\rho^+ | H^{PV} | \Delta^{++} \rangle), \tag{35c}$$

$$h_{\Delta N\rho}^1 = \sqrt{\frac{3}{2}} \langle p\rho^0 | H^{PV} | \Delta^+ \rangle + h_{\Delta N\rho}^{\prime 1} - h_{\Delta N\rho}^0, \tag{35d}$$

$$f_{\Delta\Delta\pi} = \sqrt{3} \langle \Delta^+ \rho^+ | H^{PV} | \Delta^{++} \rangle, \tag{35e}$$

TABLE II. Amplitudes for $\Delta\Delta M$ and ΔNM vertices $B \rightarrow B' + M \equiv (B'M|H^{PV}|B)$. We use the shorthand notation $A_{ij} = \alpha_{ij} + \frac{16}{3}\beta_{ij}$, $B_{ij} = \gamma_{ij} + \frac{16}{3}\delta_{ij}$, $C_{ij} = \alpha_{ij} - \frac{8}{3}\beta_{ij}$, $D_{ij} = \gamma_{ij} - \frac{8}{3}\delta_{ij}$, $E_{ij} = \alpha_{ij} - \frac{2}{3}\beta_{ij}$, $F_{ij} = \gamma_{ij} - \frac{2}{3}\delta_{ij}$, $\tilde{b}_T = b_T K^{-0.48}$, $\tilde{b}_V = b_V K^{-0.48}$, $\tilde{c}_V = c_V K^{-0.48}$, and $\tilde{y} = y \sin\theta_c \cos\theta_c$.

$\Delta^{++} \rightarrow \Delta^{++} + \rho^0$:	$2\sqrt{\frac{2}{3}}a_V(\gamma_{12} + \gamma_{22}) + \sqrt{\frac{2}{3}}a_T(-A_{11} + B_{11} + B_{12} + B_{21} + B_{12} + B_{21} + B_{22}) + \sqrt{\frac{1}{6}}(\tilde{b}_T + \tilde{b}_V)(D_{11} + D_{12} + D_{21} + D_{22})$ $+ \sqrt{\frac{1}{3}}\tilde{c}_V[-E_{11} - E_{22} - B_{11} - D_{22} - (\gamma_{12} + \gamma_{21}) - \frac{4}{3}(\delta_{12} + \delta_{21}) + 4\xi(\delta_{12} - \delta_{21})]$
$\Delta^{++} \rightarrow \Delta^{++} + \omega^0$:	$2\sqrt{\frac{2}{3}}a_V(\gamma_{11} + \gamma_{21}) + \sqrt{\frac{2}{3}}a_T(A_{11} + B_{11} + B_{12} + B_{21} + B_{22}) + \sqrt{\frac{1}{6}}(\tilde{b}_T + \tilde{b}_V)(D_{11} + D_{12} + D_{21} + D_{22})$ $+ \sqrt{\frac{2}{3}}\tilde{c}_V[-E_{11} - E_{22} - B_{11} - D_{22} - (\gamma_{12} + \gamma_{21}) - \frac{4}{3}(\delta_{12} + \delta_{21}) + 4\xi(\delta_{12} - \delta_{21})]$
$\Delta^{++} \rightarrow \Delta^+ + \rho^+$:	$\frac{2}{3}a_V\alpha_{11} + \frac{2}{3}a_T(B_{11} - B_{22}) + \frac{1}{3}(\tilde{b}_T + \tilde{b}_V)(C_{11} + D_{11} - D_{22}) + \frac{1}{3}\tilde{b}_V(-D_{12} + D_{21})$ $+ \frac{1}{3}\tilde{c}_V[-2E_{11} - E_{22} - 2B_{11} - 2F_{22} + 2(\delta_{12} + \delta_{21}) + 2\xi(\delta_{12} - \delta_{21})]$
$\Delta^{++} \rightarrow \Delta^+ + \pi^+$:	$\sqrt{\frac{1}{6}}\tilde{b}_T(-D_{12} + D_{21}) - \sqrt{3}\tilde{y}(B_{12} - B_{21}) - \sqrt{\frac{1}{6}}\tilde{c}_V[E_{22} + 2(\gamma_{12} + \gamma_{21}) + \frac{14}{3}(\delta_{12} + \delta_{21}) - 4\delta_{22} - 6\xi(\delta_{12} - \delta_{21})]$
$\Delta^{++} \rightarrow p + \rho^+$:	$\frac{4}{3\sqrt{2}}a_V\alpha_{11} + \frac{4}{3\sqrt{2}}a_T(B_{11} - B_{22}) + \frac{\sqrt{2}}{6}\tilde{b}_T(-C_{11} + 2D_{11} - 2D_{22}) + \frac{\sqrt{2}}{6}\tilde{b}_V(2C_{11} - D_{11} + D_{12} - D_{21} + D_{22})$ $+ \frac{\sqrt{2}}{3}\tilde{c}_V[-2E_{11} - E_{22} - 2B_{11} - 2F_{22} + 2(\delta_{12} + \delta_{21}) + 2\xi(\delta_{12} - \delta_{21})]$
$\Delta^+ \rightarrow p + \omega^0$:	$-\frac{8}{9}\sqrt{3}a_V\gamma_{21} - \frac{4}{9}\sqrt{3}a_T(B_{12} + B_{21}) + \frac{\sqrt{3}}{18}(\tilde{b}_T + \tilde{b}_V)(C_{11} + 2D_{12} - 4D_{21} - 2D_{22})$
$\Delta^+ \rightarrow p + \rho^0$:	$+\frac{2}{3\sqrt{3}}\tilde{c}_V[E_{22} + 2(\gamma_{12} + \gamma_{21}) + \frac{14}{3}(\delta_{12} + \delta_{21}) - 4\delta_{22} - 6\xi(\delta_{12} - \delta_{21})]$ $-\frac{8}{9}\sqrt{3}a_V\gamma_{22} - \frac{4}{9}\sqrt{3}a_T(-A_{11} + B_{11} + B_{22}) + \frac{\sqrt{3}}{18}\tilde{b}_T(3C_{11} - 4D_{11} - 2D_{12} + 2D_{22}) + \frac{\sqrt{3}}{18}\tilde{b}_V(-3C_{11} + 2D_{11} - 2D_{21} - 4D_{22})$
$\Delta^- \rightarrow \Delta^- + \omega^0$:	$+\frac{2}{3\sqrt{3}}\tilde{c}_V[2E_{11} + E_{22} + 2B_{11} + 2F_{22} - 2(\delta_{12} + \delta_{21}) - 2\xi(\delta_{12} - \delta_{21})]$ $-2\sqrt{\frac{2}{3}}a_V(-\gamma_{11} + \gamma_{21}) - \sqrt{\frac{2}{3}}a_T(-A_{11} - B_{11} + B_{12} + B_{21} - B_{22}) + \sqrt{\frac{1}{6}}(\tilde{b}_T + \tilde{b}_V)(D_{11} - D_{12} - D_{21} + D_{22})$
$\Delta^- \rightarrow \Delta^- + \rho^0$:	$+ \sqrt{\frac{2}{3}}\tilde{c}_V[-E_{11} - B_{11} - \gamma_{22} + (\gamma_{12} + \gamma_{21}) + \frac{10}{3}(\delta_{12} + \delta_{21}) - \frac{4}{3}\delta_{22} - 2\xi(\delta_{12} - \delta_{21})]$ $2\sqrt{\frac{2}{3}}a_V(\gamma_{12} - \gamma_{22}) + \sqrt{\frac{2}{3}}a_T(A_{11} - B_{11} + B_{12} + B_{21} - B_{22}) + \sqrt{\frac{1}{6}}(\tilde{b}_T + \tilde{b}_V)(-D_{11} + D_{12} + D_{21} - D_{22})$
$\Delta^- \rightarrow n + \rho^-$:	$+ \sqrt{\frac{2}{3}}\tilde{c}_V[E_{11} + B_{11} + \gamma_{22} - (\gamma_{12} + \gamma_{21}) - \frac{10}{3}(\delta_{12} + \delta_{21}) + \frac{4}{3}\delta_{22} + 2\xi(\delta_{12} - \delta_{21})]$ $-\frac{4}{3\sqrt{2}}a_V\alpha_{11} - \frac{4}{3\sqrt{2}}a_T(B_{11} - B_{22}) - \frac{\sqrt{2}}{6}\tilde{b}_T(-C_{11} + 2D_{11} - 2D_{22}) - \frac{\sqrt{2}}{6}\tilde{b}_V(2C_{11} - D_{11} - D_{12} + D_{21} + D_{22})$
$\Delta^- \rightarrow \Delta^0 + \rho^-$:	$-\sqrt{\frac{2}{3}}\tilde{c}_V[-2E_{11} - E_{22} - 2B_{11} - 2F_{22} + 2(\delta_{12} + \delta_{21}) + 2\xi(\delta_{12} - \delta_{21})]$ $\frac{2}{3}a_V\alpha_{11} + \frac{2}{3}a_T(B_{11} - B_{22}) + \frac{1}{3}(\tilde{b}_T + \tilde{b}_V)(C_{11} + D_{11} - D_{22}) + \frac{1}{3}\tilde{b}_V(D_{12} - D_{21})$ $+ \frac{1}{3}\tilde{c}_V[-2E_{11} - E_{22} - 2B_{11} - 2F_{22} + 2(\delta_{12} + \delta_{21}) + 2\xi(\delta_{12} - \delta_{21})]$

$$h_{\Delta\Delta\omega}^0 = -\frac{1}{2}\sqrt{\frac{3}{2}}(\langle\Delta^-\omega|H^{PV}|\Delta^-\rangle + \langle\Delta^{++}\omega|H^{PV}|\Delta^{++}\rangle), \quad (35f)$$

$$h_{\Delta\Delta\omega}^1 = \frac{1}{2}\sqrt{\frac{3}{2}}(\langle\Delta^-\omega|H^{PV}|\Delta^-\rangle - \langle\Delta^{++}\omega|H^{PV}|\Delta^{++}\rangle), \quad (35g)$$

$$h_{\Delta\Delta\rho}^0 = \frac{1}{2}\sqrt{\frac{2}{3}}(\langle\Delta^{++}\rho^0|H^{PV}|\Delta^{++}\rangle - \langle\Delta^-\rho^0|H^{PV}|\Delta^-\rangle) - \frac{1}{2}(\langle\Delta^+\rho^+|H^{PV}|\Delta^{++}\rangle + \langle\Delta^0\rho^-|H^{PV}|\Delta^-\rangle), \quad (35h)$$

$$h_{\Delta\Delta\rho}^1 = -\frac{1}{2}\sqrt{\frac{3}{2}}(\langle\Delta^{++}\rho^0|H^{PV}|\Delta^{++}\rangle + \langle\Delta^-\rho^0|H^{PV}|\Delta^-\rangle), \quad (35i)$$

$$h_{\Delta\Delta\rho}^2 = \frac{\sqrt{6}}{2}[\langle\Delta^+\rho^+|H^{PV}|\Delta^{++}\rangle + \langle\Delta^0\rho^-|H^{PV}|\Delta^-\rangle - \sqrt{\frac{2}{3}}(\langle\Delta^{++}\rho^0|H^{PV}|\Delta^{++}\rangle - \langle\Delta^-\rho^0|H^{PV}|\Delta^-\rangle)], \quad (35j)$$

$$h_{\Delta\Delta\rho}^{1'} = \frac{3}{4\sqrt{2}}(\langle\Delta^+\rho^+|H^{PV}|\Delta^{++}\rangle - \langle\Delta^0\rho^-|H^{PV}|\Delta^-\rangle). \quad (35k)$$

It is straightforward to evaluate the $SU(6)_w$ reduced matrix elements a_T , a_V , b_T , b_V , and c_V . Equation (8) is used to evaluate a_V and a_T . The matrix element of the axial vector between two nucleons can be taken from beta decay, and the matrix element of the vector current between a ρ and the vacuum can be obtained from e^+e^- annihilation at the ρ resonance. Values for b_T , b_V , and c_V [or equivalently \mathcal{O} of Eqs. (19) and $\langle\mathcal{O}\rangle$ of Eq. (26)] may be obtained by fitting hyperon decay amplitudes to $SU(6)_w$ predictions. The experimental values, the $SU(6)_w$ calculations, and the fitted values of these amplitudes are all given in DDH. Following this procedure, we obtained the following values for the reduced matrix elements: $a_T = a_V/3 = 1.38 \times 10^{-7}$, $b_T = -b_V = 8.85 \times 10^{-7}$, and $c_V = 6.90 \times 10^{-7}$.

Evaluation of the remaining parameters is more ambiguous. The strong-interaction parameter K is given by Eq. (34), but values for the QCD constant g , and for the renormalization point μ , are not well defined. The coefficient y is defined by Eq. (12), but there is model dependence in the choice of quark masses and in the determination of the matrix element S . The reduced matrix element ξ , which comes from a Fierz rearrangement of the $VA - AV$ terms evaluated for the sum-rule diagrams, is not well defined since we do not know the precise mechanism for generating the c_V terms.

As mentioned above, values for b_T , b_V , and c_V were obtained from experimental $\Delta S = 1$ hyperon decay amplitudes. Possible $SU(6)$ symmetry breaking will affect vector-meson vertices and pionic vertices differently as discussed in DDH. Therefore, to account for possible $SU(6)$ symmetry breaking, we introduce the parameters η and η' . For the vector-meson vertices, c_V is multiplied by η' , whereas b_T and b_V are multiplied by η . For strangeness-conserving pionic vertices, several options are discussed in DDH; in this work we choose not to scale the b_T , b_V , and c_V contributions.

Since there are considerable uncertainties for the values of some of these parameters, we have, following DDH, generated for each weak coupling both a “best value,” which is based on a defined value for each parameter, and a range, which is obtained by varying parameters over reasonable values. Our best values and approximate ranges are shown in Table III in units of 3.8×10^{-8} . The best values are obtained for the strong-interaction parameter $K=4$, the b_T , b_V , and c_V scaling factors $\eta = \eta' = 0.5$, and the reduced matrix element $\xi = 0$. For y

we use Eq. (12) with $m_u + m_d = 11.7/Z$ MeV, where Z is a renormalization factor, and $S = Z = \frac{5}{8}$, yielding $y = 4.63 \times 10^{-7}$. The ranges correspond to variations in K from 1 to 7, η from 0 to 1, η' from 0 to 1, and y from zero to its value with $S = Z = 1$ and $m_u + m_d = 11.7$ MeV, viz., $y = 1.18 \times 10^{-6}$.

In Table III we also compare these “best values” to those calculated following a similar prescription developed by Desplanques.²² The only differences between the two methods are Desplanques’ choice of $\xi = 1$, a slight change in the strong-interaction enhancement of the c_V term, and a different way of calculating the factorization contribution for the pion couplings, which is equivalent to replacing Eq. (12) with

$$y = \frac{4}{3\sqrt{2}} \frac{a_T}{\sin\theta_c \cos\theta_c}. \quad (36)$$

We have also calculated the NNM coupling constants using both our method and that of Desplanques. Those results are given in Table IV. Despite the similarity between the two methods, there are considerable differences in some of the coupling constants. Also, there is a considerable difference between our “best” values and those given in DDH due to a difference in how the “best” values are defined. Notably, our value for f_π is smaller than that of DDH, and it is more consistent with other determinations, both experimental^{2,3} and theoretical.^{5,6}

There is clearly considerable uncertainty in our predic-

TABLE III. Range and two sets of “best values” for ΔNM and $\Delta\Delta M$ effective Hamiltonian coupling constants. Values are in units of $g_\pi = 3.8 \times 10^{-8}$.

Coupling constant	Best value	Desplanques	Range
$f_{\Delta\Delta\pi}$	-20	-20	-51-0
$h_{\Delta N\omega}^1$	11	10	5-17
$h_{\Delta N\rho}^0$	20	30	-54-152
$h_{\Delta N\rho}^1$	20	20	17-26
$h_{\Delta N\rho}^{1'}$	0	0	-0.5-2
$h_{\Delta\Delta\omega}^0$	41	52	-20-85
$h_{\Delta\Delta\omega}^1$	12	11	5-18
$h_{\Delta\Delta\rho}^0$	-17	-5	-51-71
$h_{\Delta\Delta\rho}^1$	3	2	-3-8
$h_{\Delta\Delta\rho}^{1'}$	0	0	-1-3
$h_{\Delta\Delta\rho}^2$	34	34	30-45

TABLE IV. Range and three sets of “best values” for NNM effective Hamiltonian coupling constants. Values are in units of $g_\pi = 3.8 \times 10^{-8}$.

Coupling constant	Our method	Desplanques	DDH	Range
$f_{NN\pi}$	7	7	12	0–17
$h_{NN\omega}^1$	–6	–6	–3	–10––3
$h_{NN\rho}^0$	–10	–16	–30	–82–28
$h_{NN\rho}^1$	–1	–1	–0.5	–3–1
$h_{NN\rho}^2$	–18	–18	–25	–25––16

tions for these coupling constants. The ranges given are, however, very conservative, since they represent the greatest excursions from the “best” value found for the large variations taken for K , η , η' , and y . Finally, it should be emphasized that the values for the coupling constants given in Tables III and IV are not uncorrelated. The model we have used is much more predictive than the ranges given in Tables II and IV would seem to indicate since these couplings are, in fact, all determined from choosing only four parameters. The expressions given in Eqs. (35) and Table II can be used to examine the parameter dependence in more detail.

IV. CONCLUSIONS

We have carried out quark-model calculations of parity-violating weak vertices between Δ 's, nucleons, and mesons, generalizing the work of Desplanques, Donoghue, and Holstein to include the Δ sector. The quark-level Weinberg-Salam weak Hamiltonian including strong-interaction renormalization was employed. Evaluation of the relevant matrix elements of this Hamiltonian could be broken into three separate terms representing different topologies of Feynman diagrams, the “factorization” diagram, the “quark-model” diagram, and the “sum-rule” diagram. This treatment requires ten parameters. Five of these, the $SU(6)_w$ reduced matrix elements (only three of which are independent in our model), could

be related to known processes and were obtained from fits to data. A sixth, related to the pseudoscalar production of pions in the factorization term, could be estimated based on the quark equations of motion and PCAC. The others, used to approximate the effects of $SU(6)_w$ symmetry breaking, to set the scale for the strong-interaction renormalizations, and to estimate the scalar-pseudoscalar matrix elements in the sum-rule diagram, could only be estimated based on physical insight and experience in the nucleon sector. This treatment enabled us to evaluate the coupling constants for an effective one-meson-exchange parity-violating interaction involving both nucleons and Δ 's. The procedure for fitting and “guessing” the various parameters of the model led us to specify both a set of “best values” for these couplings based on the preferred values of the parameters and a set of ranges based on reasonable variations in each of the parameters. Expressions were given to allow further exploration of the parameter dependence and interrelationships between the calculated coupling constants.

The resulting effective parity-violating interaction is intended for use with models of the nucleon-nucleon interaction which include Δ degrees of freedom. It will be applied to the description of parity violation in proton-proton scattering in a subsequent publication.²³

This work is supported in part by the U.S. Department of Energy under Grant No. DE-FG02-88ER40415 and by the National Science Foundation.

¹E. M. Henley, *Annu. Rev. Nucl. Sci.* **19**, 367 (1969).

²E. G. Adelberger and W. C. Haxton, *Annu. Rev. Nucl. Part. Sci.* **35**, 501 (1985).

³B. R. Holstein, *Can. J. Phys.* **66**, 508 (1988).

⁴B. Desplanques, J. F. Donoghue, and B. R. Holstein, *Ann. Phys. (N.Y.)* **124**, 449 (1980).

⁵V. M. Dubovik and S. V. Zenkin, *Ann. Phys.* **172**, 100 (1986).

⁶N. Kaiser and Ulf-G. Meissner, *Nucl. Phys.* **A510**, 759 (1990); **A499**, 699 (1989).

⁷G. Barton, *Nuovo Cimento* **19**, 512 (1961).

⁸S. A. Page, paper presented at Lake Louise Winter Institute, Lake Louise, 1987; see also J. Birchall, G. Roy, and W. T. H. van Oers, *Phys. Rev. D* **37**, 1769 (1988).

⁹R. R. Silbar, W. M. Kloet, L. S. Kisslinger, and J. Dubach, *Phys. Rev. C* **40**, 2218 (1989).

¹⁰G. N. Epstein, *Phys. Lett.* **71B**, 267 (1977).

¹¹R. M. Gorman and B. H. J. McKellar, *Mod. Phys. Lett. A* **1**, 631 (1986).

¹²R. W. Harper, V. Yuan, H. Fraunfelder, J. D. Bowman, R. Carlini, R. E. Mischke, D. E. Nagle, R. L. Talaga, and A. B. McDonald, *Phys. Rev. D* **31**, 1151 (1985); V. Yuan, H. Fraunfelder, R. W. Harper, J. D. Bowman, R. Carlini, D. W. MacArthur, R. E. Mischke, D. E. Nagle, R. L. Talaga, and A. B. McDonald, *Phys. Rev. Lett.* **57**, 1680 (1986).

¹³W. M. Kloet, R. R. Silbar, and J. A. Tjon, *Phys. Rev. C* **41**, 2263 (1990).

¹⁴W. M. Kloet and R. R. Silbar, *Nucl. Phys.* **A338**, 281 (1980); **A364**, 346 (1981); R. R. Silbar and W. M. Kloet, *ibid.*, **A338**, 317 (1980).

¹⁵F. C. Michel, *Phys. Rev. B* **133**, 329 (1964).

¹⁶B. H. J. McKellar, *Phys. Lett.* **26B**, 107 (1967); E. Fischbach, *Phys. Rev.* **170**, 1398 (1968); D. Tadic, *ibid.* **174**, 1694 (1968);

- W. Kummer and M. Schweda, *Acta Phys. Aust.* **28**, 303 (1968).
- ¹⁷B. H. J. McKellar and P. Pick, *Phys. Rev. D* **7**, 260 (1972).
- ¹⁸We use the convention $\gamma_5 = \begin{pmatrix} 0 & -1 \\ 1 & 0 \end{pmatrix}$.
- ¹⁹K. Wilson, *Phys. Rev.* **179**, 1499 (1969).
- ²⁰D. Gross and F. Wilczek, *Phys. Rev. D* **8**, 3633 (1973).
- ²¹G. Altarelli, R. K. Ellis, L. Maiani, and R. Petronzio, *Nucl. Phys.* **B88**, 215 (1975).
- ²²B. Desplanques, *Nucl. Phys.* **A335**, 147 (1980).
- ²³J. Dubach, W. M. Kloet, and R. R. Silbar (unpublished).